JBC Papers in Press. Published on October 3, 2019 as Manuscript RA119.010568
The latest version is at http://www.jbc.org/cgi/doi/10.1074/jbc.RA119.010568

Discovery of a functional, contracted heme-binding motif within a multiheme cytochrome

Christina Ferousi[1,§,a], Simon Lindhoud[1,#,a], Frauke Baymann[2,*], Eric R. Hester[1], Joachim Reimann[1,*], Boran Kartal[3,*]

[1] Department of Microbiology, IWWR, Radboud University, Nijmegen, The Netherlands

[2] Laboratoire de Bioénergétique et Ingénierie des Protéines UMR 7281 CNRS/AMU, Marseille, France

[3] Microbial Physiology Group, Max Planck Institute for Marine Microbiology, Bremen, Germany

Running title: *Discovery of a functional contracted heme-binding motif*

Current addresses:

[§] Department of Chemistry and Chemical Biology, Cornell University, Ithaca, NY, USA

[#] Laboratory of Biochemistry, Wageningen University, Wageningen, The Netherlands

[a] These authors contributed equally to this paper

[*] corresponding authors:

Boran Kartal: bkartal@mpi-bremen.de

Microbial Physiology Group, Max Planck Institute for Marine Microbiology, Celciusstrasse 1, Bremen, Germany, bkartal@mpi-bremen.de, +49 421 2028 645

Frauke Baymann: baymann@imm.cnrs.fr

Joachim Reimann: jokelreimann@gmail.com

Keywords: anaerobic ammonium oxidation (anammox), cytochrome c, heme proteins, nitrogen cycle, EPR spectroscopy, nitric oxide (NO), hydrazine synthase (HZS), KsTH, contracted heme binding motif, tetraheme cytochrome

ABSTRACT

Anaerobic ammonium-oxidizing (anammox) bacteria convert nitrite and ammonium via nitric oxide (NO) and hydrazine into dinitrogen gas by using a diverse array of proteins, including numerous c-type cytochromes. Many new catalytic and spectroscopic properties of c-type cytochromes have been unraveled by studies on the biochemical pathways underlying the anammox process. The unique anammox intermediate hydrazine is produced by a multiheme cytochrome c protein, hydrazine synthase, through the comproportionation of ammonium and NO and the input of three electrons. It is unclear how these electrons are delivered to hydrazine synthase. Here, we report the discovery of a functional tetraheme c-type cytochrome from the anammox bacterium Kuenenia stuttgartiensis with a naturally occurring contracted Cys–Lys–Cys–His (CKCH) heme-binding motif, which is encoded in the hydrazine synthase gene cluster. The purified tetraheme protein (named here KsTH) exchanged electrons with hydrazine synthase. Complementary spectroscopic techniques revealed that this protein harbors four low-spin hexa-coordinated hemes with His/Lys (heme 1), His/Cys (heme 2), and two His/His ligations (hemes 3 and 4). A genomic database search revealed that c-type cytochromes with a contracted CXCH heme-binding motif are present throughout the bacterial and archaeal domains in the tree of life, suggesting that this heme recognition site may be employed by many different groups of microorganisms.

Introduction

Anaerobic ammonium-oxidizing (anammox) bacteria use nitrite as their terminal electron acceptor and produce dinitrogen gas (N_2). These microorganisms first reduce nitrite to nitric oxide (NO) and then use hydrazine synthase (HZS), an enzyme unique to anammox bacteria, to combine NO with ammonium to form hydrazine. HZS is a heterotrimeric protein complex that harbors two spatially separated active site hemes and catalyzes the formation of hydrazine (1, 2). In HZS,

the reductive conversion of nitric oxide (NO) yields hydroxylamine (NH_2OH), which is then combined with ammonia through a comproportionation reaction (2). The produced hydrazine is subsequently oxidized to N_2 by hydrazine dehydrogenase (HDH) (3, 4) releasing four low-potential electrons that are used for carbon fixation and the preceding catabolic reactions such as hydrazine synthesis (5, 6).

The entire HZS gene cluster (kuste2854-61) is conserved in all sequenced anammox genomes, and two of the gene products (kuste2855-56 or KSMBR1_3597-3578 in the anammox bacterium *Kuenenia stuttgartiensis*) form a membrane-associated protein complex (7, 8). This complex is suggested to form the membrane-bound, quinol-interacting electron transfer module (ETM) of HZS, and either interact directly with HZS, or work in tandem with a soluble electron carrier (5). The latter is the product of another gene from the HZS cluster (kuste2854 or KSMBR1_3596), hereafter referred to as KsTH ('Ks' standing for *Kuenenia stuttgartiensis* and 'TH' for Tetraheme). KsTH is a 236-amino-acid cytochrome *c* protein that contains three canonical heme *c* binding sites and belongs to the c_{554} protein family (9). Cytochrome c_{554} is a crystallographically resolved tetraheme *c*-type cytochrome that is suggested to accept electrons from hydroxylamine oxidation catalyzed by hydroxylamine oxidoreductase (HAO) (10, 11). C_{554} harbors three hexa-coordinated hemes (i.e., heme 1, 3, and 4 in order of appearance in the sequence) and one penta-coordinated high-spin heme center (heme 2) (12). Heme 2 of c_{554} has also been implicated in NO binding and catalysis, albeit the latter remains inconclusive (13-16).

Many reactions in the anaerobic ammonium oxidation pathway involve the activity of *c*-type cytochromes (17). Indeed, anammox bacteria encode more than 60 cytochrome *c* proteins in their genomes, and their discovery enriched our knowledge on metabolic reactions that occur in nature (1, 2, 4, 18). Investigation of the biochemical

reactions that underlie the anammox metabolism through the characterization of key enzymes has led to the discovery of novel properties of *c*-type cytochromes and the reactions they can catalyze (1-4, 18, 19). Cytochrome *c* proteins are characterized by one or more *c*-type heme cofactors that are covalently bound to the protein backbone. The two vinyl groups of a heme *b* moiety form thioether bonds with the sulfhydryls of two cysteine residues that are commonly arranged in the highly conserved amino acid sequence CXXCH, the canonical heme-binding motif (20). Although the functional implications of covalent heme attachment are not fully understood, it has been proposed that it enhances protein stability and allows for more solvent-exposed heme centers (21). The histidine residue of the CXXCH motif typically serves as the proximal ligand to the heme iron, whereas the distal ligand is often a histidine or a methionine residue at a variable distance from the motif in the amino acid sequence (22). Even though the canonical CXXCH is by far the most common heme-binding motif, several cytochromes with more than two residues separating the cysteines have been described. The most extended heme-binding motif that has been identified so far is found in octaheme MccA from *Shewanella* and several ε-Proteobacteria and contains 15 or 17 residues between the two cysteines ($CX_{15/17}CH$) (23). Several *Desulfovibrio* species express c_3 tetraheme cytochromes where one or two hemes are bound to a CX_4CH motif, and a CX_3CH motif has been observed in *Desulfovibrio gigas* (24). A CX_4CH motif is also present in hydrazine dehydrogenase (HDH) of anammox bacteria, a hydroxylamine oxidoreductase-like octaheme cytochrome *c* protein that catalyzes hydrazine oxidation to N_2 (3, 4). Although, once a functional heme-containing holoprotein protein with a contracted heme-binding motif was produced synthetically, in contrast to extensions, contractions of heme-binding motifs (i.e., CXCH or CCH) have not been observed in nature (25).

In addition to three canonical CXXCH heme-binding motifs, KsTH also contains a

CKCH sequence that is fully conserved in all 14 anammox TH sequences that were investigated in this study, and potentially serves as a fourth, contracted heme-binding site. In the current study, we addressed this hypothesis using an array of complementary methods and characterized the spectroscopic and redox properties of purified KsTH. We demonstrated that this contracted heme binding motif bound a heme *c* cofactor, we assessed whether this contracted heme coordination resulted in any distinct properties for the heme, and we probed the interaction between purified KsTH and hydrazine synthase.

Results and Discussion

KsTH harbors four c-type heme cofactors

The gene product of kuste2854 was purified directly from *K. stuttgartiensis* biomass by a three-step purification protocol. The purified protein migrated as a monomeric species on both native and SDS-denaturing PAGE. Peptide mass fingerprinting using MALDI-TOF mass spectrometry verified the identity of the protein as kuste2854. Tandem mass spectrometry analysis of the intact, albeit denatured full-length protein established a molecular mass of 26095.3 Da for the monoisotopic species (Figure 1A). The theoretical value of the apoprotein without the N-terminal targeting sequence (aa: 1-29) was 23634.79 Da. The +2460.4844 Da offset in mass could only be explained by the covalent binding of four heme groups to the protein backbone, resulting in a total theoretical mass of 26095.46 Da for the holoprotein, which was an exact match to the mass measured for the denatured full-length protein. Collision-induced dissociation tandem mass spectrometry (CID MS/MS) detected only one dominant fragment ion of 617.18 $[M+H]^{1+}$ Da, and its spectrum matched the simulated isotope envelope of Fe-protoporphyrin IX (heme *b*) (Figure 1B). Consequently, the observed mass discrepancy was most likely due to the covalent attachment of four heme groups instead of the three that were predicted from the presence of three canonical CXXCH heme *c* binding motifs in the KsTH

sequence. Hence, this additional heme must be bound to a non-canonical heme-binding motif. Apart from the cysteine residues present in the three canonical heme binding sites, there are four additional cysteines present in the KsTH sequence (Cys12, Cys14, Cys20, and Cys151). Only two of these cysteine residues could constitute a heme-binding site, the contracted CKCH motif, which has been designated as 'Heme 1 binding site' (Figure 2).

To probe the covalent attachments formed between the heme moieties and the protein backbone, the reduced alkaline pyridine hemochromogen spectrum of KsTH was recorded. Bis–pyridine heme adducts that are linked to the protein via two thioether bonds result in an absorbance maximum of the alpha band at 550 nm, whereas the presence of only a single thioether bond results in a red–shifted maximum at 553 nm (26). In perfect agreement, the reduced alkaline bis–pyridine adduct of KsTH displayed the typical absorbance maximum at 550 nm (Figure 3), which was indicative of two thioether bonds linking the heme to the protein backbone (26). Taken together, these results further corroborated that the CKCH motif served as the additional heme-binding site in KsTH.

All four hemes are low-spin and hexa-coordinated

Visible and electron paramagnetic resonance (EPR) spectroscopy were used to investigate the spin state of the KsTH hemes as well as the nature of their ligation. In optical spectroscopy, oxidized high-spin hemes with a single axial ligand exhibit a Soret maximum around 390 nm and a charge transfer absorption band around 600 nm, whereas in the reduced state a broad signal around 430 nm is generally observed (13, 27). Neither of these two features were observed in the KsTH spectra (Figure 4). In EPR spectroscopy high-spin hemes give rise to a strong signal centered at g=6 (27, 28), which was absent from EPR spectra of KsTH recorded under different conditions (Figure 5). Interactions between a high spin heme and a neighboring co-factor can result in spectral features different from the g=6

signal. In the case of a multi-heme protein such as KsTH these interaction signals are situated between the signals of the individual hemes. For example, such a signal is observed for c_{554} at g=3.9. Nothing similar could be observed for KsTH. Furthermore, the EPR spectrum of KsTH was very similar to the spectrum of c_{554} at pH 12, where all hemes of c_{554} have been shown to be low-spin (30).

Heme axial ligation is inferred based on spectroscopy and sequence homology

The UV/Vis electronic absorption spectrum of the as-isolated (fully oxidized) KsTH displayed a broad Soret band with a maximum at 409 nm while, upon reduction, the Soret band maximum shifted to 418 nm with a pronounced increase in amplitude and decrease in half width. Absence of a shoulder at 437 nm and 564 nm (Figure 4A) ruled out the possibility of a hydroxide ligand for any of the hemes of KsTH (31) and absence of a charge transfer band at 695 nm most likely excluded methionine as a heme axial ligand (27). Upon reduction, the Soret bands of His/Lys, His/His, and His/Cys ligated hemes shift from 408 nm to 417 nm (32), 407 nm to 420 nm (30), and 418 nm to 416 nm (33), respectively. Although thiolate heme ligation in the ferric form usually exhibits red-shifted Soret bands around 418 nm (34), superposition of the optical contribution from a His/Cys ligated heme to spectra of His/His and/or His/Lys ligated hemes could account for the broad Soret band of oxidized KsTH and the pronounced narrowing and rise in the Soret band upon reduction. EPR spectroscopic studies on purified KsTH agreed with the above conclusions. The EPR spectrum of oxidized KsTH at 15 K had broad spectral features in the g=2.67 to g=1.74 range that relaxed slowly. The shape of these signals slightly narrowed at higher temperature, above 70 K (Figure 5A). The broad shape and temperature-dependent behavior were both characteristic of a spin-spin interacting system of low-spin hemes. This was consistent with the EPR spectra of another tetraheme *c*-type cytochrome, cytochrome c_{554}, where pairwise interaction between

hemes 1 and 3 and hemes 2 and 4 induced interaction signals in EPR (29). Partial reduction of the sample by small amounts of dithionite induced disappearance of the interaction signal and the appearance of two heme signals (Figure 5B). One of these had a g_z-value of 3.28, characteristic of highly anisotropic low-spin hemes with His/Lys or His/His ligation (27). The other signal features g values at 2.54, 2.29, and 1.84, which were compatible with a His/Cys ligated oxidized heme (33, 35, 36).

In order to retrieve more information about KsTH based on its primary structure, homology searches were performed against non-redundant protein sequences using BlastP. While there was no significant hit to any characterized homolog, a conserved domain belonging to the c_{554} protein family was identified (9). This domain was found close to the C-terminus and accounted for approximately one third of the total KsTH sequence length (i.e., amino acids 41-110). Multiple sequence alignments of KsTH orthologs with cytochrome c_{554} (Figure 2) combined with structural insights from the tertiary structure of c_{554} allowed us to assign the above-mentioned identified heme ligations to specific hemes. For two of the hemes, the ligands that were detected in KsTH using EPR spectroscopy, could be identified in the amino acid sequence of the protein by sequence alignment between anammox TH and c_{554}. They were conserved between all TH sequences from all known anammox species and situated within the stretch that was homologous to c_{554}. The distal histidine ligand to heme 4 was conserved among c_{554} and TH (His30), and in TH there was a fully conserved lysine residue (Lys97) instead of the distal histidine ligand of heme 1 of c_{554}. The His ligand to heme 3 of c_{554} was outside the protein sequence which was homologous to TH. However, in addition to the above discussed His ligands, there was only one further histidine fully conserved in TH sequences which was likely the sixth ligand to heme 3.

As discussed above, all hemes of KsTH had two axial ligands, while heme 2 of c_{554} had only one. Based on the sequence

alignment of KsTH with the structure of c_{554} we predicted a stretch of 6 amino acids (aa: 147-152) at the distal side of heme 2 of KsTH. This loop was fully conserved in all sequenced anammox genomes and contained one cysteine and three lysine residues that could potentially serve as iron ligands. EPR and UV-VIS spectroscopy points towards the presence of a Cys-ligated heme and we therefore propose Cys150 as the sixth ligand for heme 2 in KsTH. Taken together, our results showed that KsTH harbored four hexa-coordinated hemes with His/Lys (heme 1), His/Cys (heme 2), and two His/His ligations (heme 3 and heme 4).

KsTH hemes have low redox midpoint potentials

To assess the redox properties of the heme cofactors of KsTH electrochemical redox titration monitored by optical spectroscopy was performed (Figure 6). KsTH titrated in two waves, one centered around -200 mV (*vs.* SHE) accounting for 66-85% of the total signal amplitude and the remaining 15-33% around -400 mV (*vs.* SHE).

EPR spectra recorded on samples prepared at a few selected potentials between the fully oxidized TH and -400 mV (Figure 5B) showed characteristic individual EPR signatures for two of the hemes and interactions signatures at higher potentials when all four hemes were oxidized.

The three hemes of the high-potential wave (-200 mV) exhibited slightly different redox midpoint potentials. Reduction of the highest potential heme induced loss of its interaction with the neighboring heme and, therefore, appearance of a signal at g=3.28 (pair of hemes 1 and 3). Further decrease of the potential first brought up the signal of the Cys ligated heme (heme 2) due to reduction of its interacting partner (heme 4), and then induced disappearance of the g=3.28. The low-potential wave (-400 mV) could be attributed to the Cys ligated heme, which could only be partially reduced by dithionite. Such low redox midpoint potentials have been reported earlier for His/Cys-ligated hemes (33, 35).

In optical spectroscopy the difference spectra of the hemes contributing to the

transition at -200 mV could not be resolved. The spectrum showed an α band maximum at 552 nm and a Soret band at 418 nm. The spectrum of the low-potential component exhibited a blue-shifted α band at 549 nm accompanied by a split Soret band with a maximum at 418 nm and a shoulder at 425 nm (Figure 6B). Splitting of variable intensity was observed, depending on the sample preparation and the redox direction. A possible explanation for the variability of these spectroscopic signals could involve either conformational changes around the heme pocket and/or ligand exchange of the respective heme iron that might have occurred upon electrochemical reduction. An interesting case of redox-dependent ligand change has been reported for cytochrome *c*'' from *Methylophilus methylotrophus* in which the detachment of the distal histidine ligand upon reduction leads to spin-state transition (37). Additionally, in the alkaline conformer of mitochondrial cytochrome *c* the native methionine distal ligand of the heme iron is replaced by a lysine (34).

Heme environments are flexible: external ligands can bind to the hemes

To further examine the heme ligand environment, potential external ligands were added to KsTH. Upon addition of CO to the reduced protein, 75% of the α band changed its shape, indicating that CO became a ligand to three out of four hemes (Figure 4B). The Soret band became narrower but, unexpectedly, did not increase in amplitude. Addition of a ~9-fold excess of NO/heme (600 μM NO for 65 μM heme) to the oxidized protein resulted in an optical spectrum of NO-bound heme (Figure 4C) and in loss of all EPR features (Figure 5C). Upon addition of an equimolar amount of NO, the EPR signal amplitude diminished by a factor of two (Figure 5C). The reaction of NO with reduced TH was rapid as judged from the instant color change of the sample upon addition of NO-saturated buffer, even though extreme conditions such as low or high pH or incubation with high concentration of NO or CO for hours are usually necessary to

achieve NO and CO binding to reduced and oxidized cytochrome *c*, respectively (38, 39). Binding of NO to an oxidized heme can pull an electron from the heme iron resulting in loss of its paramagnetic properties. Our results suggested that NO became a ligand to all hemes of oxidized KsTH. However, exposure of pre-reduced KsTH to NO resulted in loss of the α band, corresponding to approximately two thirds of the hemes and concomitant appearance of a typical signal for NO-bound heme at 540/560 nm (Figure 4D). A heme-NO signal appeared in EPR accounting for less than one heme. The lines of the hyperfine split signal were separated by 17 Gauss indicating that NO was bound as a fifth ligand to a reduced heme (Figure 4C). Otherwise, the EPR spectra were nearly featureless, indicating that the NO-bound hemes were oxidized, except for the above-mentioned NO-heme signal around g=2 which could be a degradation product. NO, therefore, partially oxidizes KsTH with an unknown reaction product. Whether this reaction is of physiological importance remains to be determined. Additions of either imidazole or azide to the reduced protein did not result in observable spectroscopic changes.

KsTH and hydrazine synthase exhibit redox interaction

TH is conserved within the hydrazine synthase gene cluster across all sequenced anammox genomes and was hypothesized to provide three electrons for the first half-reaction of hydrazine synthesis, i.e. NO reduction to hydroxylamine (5). Therefore, electron transfer from KsTH to HZS was assessed. In a double-compartment cuvette, reduced KsTH and oxidized HZS gave rise to a Soret band at 415 nm with a shoulder at 425 nm, and an α band at 552 nm (Figure 7A), in agreement with the simulated combined spectrum. Mixing of the two enzymes resulted in loss of the shoulder at 425 nm and in the appearance of Soret band maxima at 409 and 417 nm. The 417 nm absorbance decreased over a time period of ten minutes accompanied by a shift of 409 nm band to 407 nm.

EPR spectra on a 1:1 mixture of reduced KsTH and oxidized HZS (Figure 7B) resulted in loss of lines in the g=3 region due to reduction of the corresponding heme(s) of HZS. The g=2.54 signal of the Cys ligated heme 2 and the g=3.28 signal of either heme 1 or 3 of KsTH appeared. Disappearance of the shoulder at 425 nm together with the rise of the g=2.54 signal revealed oxidation of the low-potential heme of KsTH. Subsequent shift of the Soret band maximum from 409 to 407 nm indicated further oxidation of TH. Indeed, oxidized TH exhibited a blue–shifted Soret band maximum at 407 nm compared to HZS at 409 nm. This observation was corroborated by the g=3.28 signal of oxidized heme 1 or 3 that arose in EPR spectra. Therefore, about two electrons were transferred from KsTH to HZS, resulting in the rapid oxidation of heme 2 and the subsequent slower oxidation of either heme 1 or 3.

Contracted heme-binding motifs are present in a variety of genomes

The discovery of a naturally occurring contracted heme-binding motif in TH prompted us to investigate whether contracted binding sites also occurred in proteins other than KsTH and its orthologs. We found 107 multiheme proteins that also contained the CXCH motif, which were widely spread across different phyla and present in both Archaea and Bacteria (Figure 8; Supplementary Table 1), including environmentally-relevant microorganisms such as nitrate-dependent anaerobic methane-oxidizing archaea (40, 41) and aerobic methanotrophic and methylotrophic bacteria (42). The residue separating the cysteines of the CXCH seemed to be conserved within phylogenetic groups, however, this was not the case for all groups. Notably, apart from the K residue being conserved within the anammox group, within the Desulfuromonadales group (containing the Geobacteraceae and Desulfuromonadaceae families) either a G or S residue was conserved. Nonetheless, the prevalence of this contracted motif across more than ten

phyla from both Archaeal and Bacterial domains indicated that it was not limited to anammox bacteria. Whether the divergent Cys-separating residues confer different properties is still an open question.

Conclusions

Here we characterized KsTH, a tetraheme cytochrome with one contracted CXCH heme-binding motif. Our results, combined with detailed analyses of the parts of KsTH protein sequence homologous to cyt c_{554}, allowed us to attribute ligands, redox midpoint potentials, and spectral properties to the individual hemes (numbered by order of appearance in the sequence). Hemes 1 and 3 as well as hemes 2 and 4 were in magnetic interaction, indicating that the four hemes were arranged in plan-parallel pairs. Heme 1 was attached to the protein backbone via a CKCH motif and was the first observed naturally occurring representative of such a contracted heme-binding sequence. The CXCH heme-binding motif was conserved among anammox species and our extensive database search revealed the presence of such a motif in cytochromes of a wide variety of phyla. In anammox bacteria, the heme attached to the contracted heme-binding site was His/Lys coordinated and in KsTH it exhibits a redox midpoint potential of around -200 mV (*vs.* SHE). Its interaction partner, heme 3, had roughly the same redox midpoint potential and was His/His ligated. Both hemes had an α band maximum at 418 nm and a Soret band at 552 nm and one of them had an EPR signal at g=3.28. Heme 4, belonging to the second heme pair together with heme 2, had the same optical spectrum and midpoint potential as mentioned above and it was His/His ligated. Heme 2 had a redox midpoint potential of -400 mV, probably induced by its His/Cys ligation, and features EPR signals at g=2.54/2.29/1.84. It had a distinctive optical spectrum with a Soret band at 418 and 425 nm and an α band at 549 nm. The protein environment of this heme appeared to be flexible since the split of the Soret band varied as a function of experimental conditions and the presence of

hydrazine synthase. In line with the hypothesis that TH could be an electron donor to HZS, electron transfer from reduced TH to oxidized HZS was observed. The first intermolecular one-electron transfer was rapid, whereas electron transfer from a second heme (either 1 or 3) took several minutes. Interestingly, unlike other *c*-type cytochromes, addition of NO to KsTH resulted in NO binding to all hemes and in complete oxidation of KsTH when NO was added to the reduced protein. Spectroscopic analyses of KsTH together with the presence of contracted heme-binding motifs in a diverse group of microbial phyla suggest that such unusual cytochrome *c* proteins might have more functions in nature than just shuttling electrons.

Experimental Procedures

All chemicals used were purchased from Sigma-Aldrich, unless stated otherwise. High-performance liquid chromatography (HPLC)-grade chemicals were purchased from Baker, USA. All purification steps took place in ambient air and at 4°C.

Cell-free extract preparation

Cells from a 10-liter laboratory scale enriched (~95% pure) *K. stuttgartiensis* continuous membrane bioreactor (43) were harvested and concentrated by centrifugation at 4,000 x g for 15 min (Allegra X-15R, Swinging Bucket Rotor, Beckman Coulter). The pellet was resuspended with one volume of 20 mM Tris-HCl, pH 8.0. Cells were lysed by three subsequent passages through a French Pressure Cell operating at 120 MPa (American Instrument Company). Centrifugation at 4,000 x g for 15 min (Allegra X-15R, Swinging Bucket Rotor, Beckman Coulter) removed cell debris and the obtained supernatant was subjected to ultracentrifugation at 126,000 x g for 1 h (Optima XE90, Fixed angle 90 Ti rotor, Beckman Coulter) to pellet cell membranes. The supernatant after ultracentrifugation constituted the cell-free extract.

Protein purification

KsTH (KSMBR1_3596) was brought to homogeneity in a three-step purification procedure. Cell-free extract was first fractionated with ammonium sulfate at 85% saturation. After stirring for about 1 h, the sample was let to settle overnight. The supernatant was collected by centrifugation (4,000 x g for 20 min) and diluted to about 5% ammonium sulfate saturation with 20 mM KPi, pH 7.0. Liquid chromatography was performed on an Äkta Purifier (GE Healthcare). The sample of interest was loaded onto a 30-ml column packed with Ceramic Hydroxyapatite (Bio-Rad) and equilibrated with 20 mM KPi, pH 7.0. The column was packed at a flow rate of 10 $mL \cdot min^{-1}$ (XK 26/20 column, GE Healthcare) and eluted at 5 $mL \cdot min^{-1}$; the eluate was monitored at 280 nm. KsTH eluted as a near-symmetrical peak during a 30-min linear gradient (20-500 mM KPi, pH 7.0) at a conductivity of about 40 $mS \cdot cm^{-1}$. This peak was collected and concentrated with 10-kDa molecular mass cut-off polyethersulfone spin filters (Vivaspin 20; Sartorius Stedim Biotech). The concentrated sample was subsequently loaded on a 65-ml column packed with Superdex 200 (GE Healthcare) and equilibrated with 50 mM KPi, 150 mM NaCl, pH 7.0. The column was packed at a flow rate of 3 $mL \cdot min^{-1}$ (XK 26/20 column, GE Healthcare) and eluted at 1 $mL \cdot min^{-1}$. Purity was checked throughout purification by SDS-denaturing polyacrylamide gel electrophoresis (PAGE) (44). The identity of the protein was established by MALDI-TOF mass spectroscopy (Bruker Biflex III, Bruker Daltonik). Enzyme preparations were either used immediately or rapidly frozen in liquid nitrogen before storage.

Electronic Absorbance Spectra

All solutions were prepared freshly in serum bottles sealed with rubber stoppers and made anoxic by alternately applying vacuum and Argon for seven times. UV-Visible spectra were recorded at room temperature in 1.4-ml or 0.2-mL quartz cuvettes (path length 1 cm; Hellma), sealed with rubber stoppers, using a Cary 60

(Agilent) that was placed inside an anaerobic glove box (N_2/H_2 atmosphere; O_2 <2 ppm) or on a Safas spectrophotometer (Société Anonyme de Fabrication d'Appareillages Scientifiques) connected to the interior of the glove box by an optical fiber. Spectra taken outside the glove box were recorded on a Cary 60 or Cary 4000 spectrophotometer (Agilent).

Addition of external ligands

NO-containing stock solution (0.9 mM) was prepared by sparging anoxic MOPS buffer (20 mM, pH 7.0) with an NO-He gas mixture (1:1, v/v) for 10 min. CO was added by directly flushing the assay cuvette with pure CO gas for 30 sec. Imidazole and azide were added from 100-fold concentrated stock solutions made with the corresponding assay buffer. To prepare reduced KsTH in the presence of NO for EPR spectroscopy an excess of dithionite was added to the EPR tube in the glove box followed by some grains for nitrite. The sample was frozen in the glove box. For the redox interaction experiment between KsTH and HZS, HZS was purified as described previously (1), and a double–chamber quartz cuvette was used (path length 0.875 cm; Hellma Analytics) under the same conditions described above.

Interaction with Hydrazine synthase

5 equivalents of KsTH and 1 equivalent of HZS were added in two separated compartments of a double compartment cell. Optical spectra were recorded on the oxidized proteins and after successive additions of dithionite, until KsTH was completely reduced without excess of reductant being present in the cell. Their combined static spectra were recorded and, following mixing, three spectra of the merged samples were recorded with 3 min interval time. Upon mixing, the maximum intensity of the reduced Soret region decreased, which confirmed the absence of any excess reductant in the cell. Fully reduced KsTH (without excess of reductant) was prepared in a glove box and mixed with oxidized HZS in a 1:1 stoichiometry for EPR spectroscopy.

Electrochemical redox titration

Redox titrations of purified KsTH were performed with a modified version of the optically transparent thin-layer electrochemical cell (OTTLE) originally designed by the workshop of the physical chemistry department of the University Freiburg (45). The OTTLE was connected to a potentiostat (PGSTAT204, Metrohm Autolab) and the spectroscopic changes of the sample upon potentiometric titration were monitored from 400 to 610 nm using a Cary 60 spectrophotometer (Agilent). The Ag/AgCl reference electrode was calibrated against a saturated quinhydrone solution in 1 M MOPS buffer, pH 7.0, at room temperature ($E^{o'}$= +280 mV) (46). The assay mixture contained 20 µM as-isolated fully oxidized KsTH in 50 mM MOPS, pH 7.0, containing 50 mM KCl, 40 mM glucose, 10U glucose oxidase, and 5U catalase. The following redox mediators were added at 20 µM final concentration each: ferrocene ($E^{o'}$= +640 mV), ferricyanide ($E^{o'}$= +430 mV), 1.4-benzoquinone ($E^{o'}$= +280 mV), 2,5-dimethyl-1,4-benzoquinone ($E^{o'}$= +180 mV), 1,2-naphtoquinone ($E^{o'}$= +145 mV), phenazine methosulfate ($E^{o'}$= +80 mV), 1,4-naphtoquinone ($E^{o'}$= +60 mV), phenazine ethosulfate ($E^{o'}$= +55 mV), 5-hydroxy-1,4-naphtoquinone ($E^{o'}$= +30 mV), 1,2-dimethyl-1,4-naphtoquinone ($E^{o'}$= 0 mV), 2,5-dihydroxy-p-benzoquinone ($E^{o'}$= -60 mV), 5,8-dihydroxy-1,4-naphtoquinone ($E^{o'}$= -145 mV), 9,10-anthraquinone ($E^{o'}$= -184 mV), 9,10-anthraquinone-2-sulfonate ($E^{o'}$= -225 mV), benzyl viologen ($E^{o'}$= -350 mV), and methyl viologen ($E^{o'}$= -440 mV/-772 mV). Titrations were performed from -475 mV to +290 mV (*vs.* SHE) at room temperature, both in reductive and oxidative directions, with potential increments of 30 mV. Equilibration time was 10 min per step. Spectral changes were evaluated on the basis of the Soret band at 418 and 425 nm and the α band at 552 and 549 nm. The midpoint redox potentials were determined by fitting the amplitude of the signal to a sum of two single electron Nernst

components using the Origin version 9.1 program (OriginLab Corp).

EPR spectroscopy

Samples were prepared in an anaerobic glove box at 65 μM heme, loaded into quartz EPR tubes sealed with butyl rubber stoppers, and then frozen in a cold finger inside the glove box. EPR spectra were recorded on α Elexsys E500 X-band spectrometer (Bruker) fitted with a He-cryostat ESR900 (Oxford Instrument) and temperature control system. Spectra were recorded under conditions given in the figure legends. Several scans were accumulated to increase the signal/noise ratio.

Redox control samples were prepared in a glove box under optical control. Small amounts of 20 mM dithionite solution prepared in 1M MOPS buffer, pH 7.0, were added to the sample until the optical spectra showed the desired change in the absorbance of the α band. An aliquot of this sample was then transferred to an EPR tube and frozen in the glove box. In a second experiment the samples were transferred back to the cuvette, 5 mM EDTA and redox mediators (same type and concentration as used for optical redox titrations; see above) were added and the potential was monitored by a redox electrode calibrated against a saturated quinhydrone solution in 1 M MOPS buffer, pH 7.0. Potential was adjusted by addition of small amounts of 20 mM dithionite solution in MOPS buffer pH 7.0, or 10 mM ferricyanide solution in water. At various potentials (-145 mV, -200 mV, -410 mV, -286 mV, -225 mV) an aliquot of the sample was transferred to an EPR tube and frozen inside the glove box.

Protein Sequence Analyses

Protein sequence homology searches were performed against selected entries using the BlastP program at the NCBI website. N-terminal signal cleavage sites were predicted with SignalP 4.1 (47). Multiple sequence alignments were performed using Muscle (48) as implemented in the EMBL web server and then manually curated.

Mass spectrometry

Samples for matrix-assisted laser desorption ionization time-of-flight (MALDI-TOF) mass spectrometry were prepared as described previously (49). Each spectrum (900–4,000 m/z) was analyzed using the Mascot Peptide Mass Fingerprint (Matrix Science) against the *K. stuttgartiensis* database, allowing methionine oxidation as variable modification, 0.2-Da peptide tolerance, and at most one trypsin mis-cleavage.

Samples for ultrahigh resolution quadrupole time-of-flight (UHR-qTOF) mass spectrometry were prepared as follows. Purified protein sample buffer was exchanged for 0.1% formic acid 20% methanol using 3 kDa molecular weight cut-off filters (Amicon Ultracel) and subsequently analyzed by direct infusion electrospray ionization tandem mass spectrometry (ESI-MS/MS) using an ultrahigh resolution quadrupole time-of-flight mass spectrometer (maXis 5G, Bruker Daltonics). The instrument was operated in positive ionization mode with the following parameters: capillary voltage: 4500 V, offset: 500 V, nebulizer gas pressure: 0.4 bar, N_2 drying gas: 4L·min^{-1} at 200°C, in-source CID energy: 20 eV, mass range 300-3,700 m/z, 1 Hz acquisition rate. The z=31$^+$ precursor ion (m/z 843.3) was isolated and subsequently fragmented using 25 eV collision induced dissociation (CID) energy. Acquired data was processed in Data Analysis 4.2 software (Bruker Daltonics). Spectral peak detection and charge deconvolution for MS and MS/MS spectra was performed by the SNAP2 algorithm. In addition, a high-resolution charge-deconvoluted MS spectrum was generated using the maximum entropy charge deconvolution algorithm (MaxEnt) which was compared to a simulated isotope pattern of KsTH (AA 30-236) plus four heme groups. The processed MS/MS spectrum was exported to BioTools 3.2 and compared against *in silico* b- and y-fragment ion masses of KsTH (AA 30-236) plus four heme groups (0.05 Da mass tolerance).

Other analytical methods

Protein concentrations were measured with the Bio-Rad protein assay, based on the method of Bradford (50), using bovine serum albumin as standard. The pyridine hemochrome assay was performed as described previously (51).

Bioinformatic analyses

The NCBI non-redundant (nr) database and all publicly available genomes from the NCBI were surveyed for the contracted heme-binding motif. Sequences that contained a CXCH motif, while also containing a CXXCH motif were retrieved. Sequences were excluded if the CXCH motif was CCCH, CXCCH, or CCXCH. SignalP 4.1 (47) was used to predict if the sequence contained a signal peptide. Positive hits that also contained a signal peptide were manually curated to exclude (i) sequences of which either the annotation excluded that they were c-type cytochromes, (ii) sequences in which the contracted motif falls within the signal sequence, (iii) sequences in which the contracted motif overlapped with the canonical motif (i.e., either CXCHXCH or CXXCHCH). The lineage of the organism in which the protein originated was obtained using the Entrez efetch protocol via the Entrez python package. In order to investigate the phylogenetic relationship of taxa containing the contracted heme-binding motif, their genomes were downloaded from the NCBI database for phylogenetic analysis. The UBCG pipeline was used to extract conserved phylogenetic marker genes and build multiple alignments (52). A final concatenated alignment of the marker genes was used to infer the phylogenetic relationship of the taxa and visualized as an unrooted tree using the Interactive Tree of Life software (53).

Acknowledgements

We thank Wolfgang Nitschke for insightful discussions. Guylaine Nuijten is acknowledged for maintenance of the *K. stuttgartiensis* culture. We thank MSM Jetten (MSMJ) for discussions and support. We acknowledge Hans Wessels for carrying out the MS/MS analysis. C.F. is supported by a Spinoza Prize awarded to M.S.M.J. by the Netherlands Organization for Scientific Research [NWO 62001581, 2012], S.L. by [NWO 824.15.011, 2015, to B.K.], B.K. by the European Research Council [ERC 640422, 2014]. J.R. by [ERC 339880, 2014, to M.S.M.J.]. This research was support by a van Gogh travel grant from EP-Nuffic and Campus France awarded to M.S.M.J. [BA/GP.16/23] and F.B. EPR work was supported by TGE RPE FR3443.

Conflict of interest

The authors declare that they have no conflicts of interest with the contents of this article.

Author contributions

CF, SL, FB, JR and BK designed the experiments. CF, SL, FB performed protein purification, identification, and spectroscopic analyses. ERH performed the database search and phylogenetic tree construction. All authors interpreted the results and contributed to the writing of the manuscript.

References

1. Kartal, B., Maalcke, W. J., de Almeida, N. M., Cirpus, I., Gloerich, J., Geerts, W., Op den Camp, H. J., Harhangi, H. R., Janssen-Megens, E. M., Francoijs, K. J., Stunnenberg, H. G., Keltjens, J. T., Jetten, M. S., and Strous, M. (2011) Molecular mechanism of anaerobic ammonium oxidation. *Nature* **479**, 127-130
2. Dietl, A., Ferousi, C., Maalcke, W. J., Menzel, A., de Vries, S., Keltjens, J. T., Jetten, M. S., Kartal, B., and Barends, T. R. (2015) The inner workings of the hydrazine synthase multiprotein complex. *Nature* **527**, 394-397
3. Maalcke, W. J., Reimann, J., de Vries, S., Butt, J. N., Dietl, A., Kip, N., Mersdorf, U., Barends, T. R., Jetten, M. S., Keltjens, J. T., and Kartal, B. (2016) Characterization of Anammox Hydrazine Dehydrogenase, a Key N_2-producing Enzyme in the Global Nitrogen Cycle. *The Journal of biological chemistry* **291**, 17077-17092
4. Akram, M., Dietl, A., Mersdorf, U., Prinz, S., Maalcke, W., Keltjens, J., Ferousi, C., de Almeida, N. M., Reimann, J., Kartal, B., Jetten, M. S. M., Parey, K., and Barends, T. R. M. (2019) A 192-heme electron transfer network in the hydrazine dehydrogenase complex. *Science Advances* **5**, eaav4310
5. Kartal, B., de Almeida, N. M., Maalcke, W. J., Op den Camp, H. J., Jetten, M. S., and Keltjens, J. T. (2013) How to make a living from anaerobic ammonium oxidation. *FEMS microbiology reviews* **37**, 428-461
6. Hu, Z., Wessels, H. J. C. T., van Alen, T., Jetten, M. S. M., and Kartal, B. (2019) Nitric oxide-dependent anaerobic ammonium oxidation. *Nature Communications* **10**, 1244
7. de Almeida, N. M., Wessels, H. J., de Graaf, R. M., Ferousi, C., Jetten, M. S. M., Keltjens, J. T., and Kartal, B. (2016) Membrane-bound electron transport systems of an anammox bacterium: A complexome analysis. *Biochim Biophys Acta* **1857**, 1694-1704
8. Frank, J., Lucker, S., Vossen, R., Jetten, M. S. M., Hall, R. J., Op den Camp, H. J. M., and Anvar, S. Y. (2018) Resolving the complete genome of *Kuenenia stuttgartiensis*

from a membrane bioreactor enrichment using Single-Molecule Real-Time sequencing. *Sci Rep* **8**, 4580

9. Sonnhammer, E. L., Eddy, S. R., and Durbin, R. (1997) Pfam: a comprehensive database of protein domain families based on seed alignments. *Proteins* **28**, 405-420

10. Hooper, A. B., Vannelli, T., Bergmann, D. J., and Arciero, D. M. (1997) Enzymology of the oxidation of ammonia to nitrite by bacteria. *Antonie van Leeuwenhoek* **71**, 59-67

11. Arp, D. J., Chain, P. S. G., and Klotz, M. G. (2007) The Impact of Genome Analyses on Our Understanding of Ammonia-Oxidizing Bacteria. *Annu. Rev. Microbiol.* **61**, 503-528

12. Yamanaka, T., and Shinra, M. (1974) Cytochrome *c*-552 and cytochrome *c*-554 derived from *Nitrosomonas europaea*. Purification, properties, and their function in hydroxylamine oxidation. *Journal of biochemistry* **75**, 1265-1273

13. Arciero, D. M., Collins, M. J., Haladjian, J., Bianco, P., and Hooper, A. B. (1991) Resolution of the four hemes of cytochrome *c*554 from *Nitrosomonas europaea* by redox potentiometry and optical spectroscopy. *Biochemistry* **30**, 11459-11465

14. Iverson, T. M., Arciero, D. M., Hooper, A. B., and Rees, D. C. (2001) High-resolution structures of the oxidized and reduced states of cytochrome *c*554 from *Nitrosomonas europaea*. *Journal of biological inorganic chemistry : JBIC : a publication of the Society of Biological Inorganic Chemistry* **6**, 390-397

15. Upadhyay, A. K., Hooper, A. B., and Hendrich, M. P. (2006) NO reductase activity of the tetraheme cytochrome *c*554 of *Nitrosomonas europaea*. *J Am Chem Soc* **128**, 4330-4337

16. McGarry, J. M., and Pacheco, A. A. (2018) Upon further analysis, neither cytochrome *c*554 from *Nitrosomonas europaea* nor its F156A variant display NO reductase activity, though both proteins bind nitric oxide reversibly. *Journal of biological inorganic*

chemistry : JBIC : a publication of the Society of Biological Inorganic Chemistry **23**, 861-878

17. Kartal, B., and Keltjens, J. T. (2016) Anammox Biochemistry: a Tale of Heme *c* Proteins. *Trends Biochem Sci* **41**, 998-1011

18. Maalcke, W. J., Dietl, A., Marritt, S. J., Butt, J. N., Jetten, M. S., Keltjens, J. T., Barends, T. R., and Kartal, B. (2014) Structural basis of biological NO generation by octaheme oxidoreductases. *The Journal of biological chemistry* **289**, 1228-1242

19. Ukita, S., Fujii, T., Hira, D., Nishiyama, T., Kawase, T., Migita, C. T., and Furukawa, K. (2010) A heterodimeric cytochrome c complex with a very low redox potential from an anaerobic ammonium-oxidizing enrichment culture. *FEMS Microbiol Lett* **313**, 61-67

20. Kranz, R. G., Richard-Fogal, C., Taylor, J. S., and Frawley, E. R. (2009) Cytochrome *c* biogenesis: mechanisms for covalent modifications and trafficking of heme and for heme-iron redox control. *Microbiol Mol Biol Rev* **73**, 510-528, Table of Contents

21. Kleingardner, J. G., and Bren, K. L. (2015) Biological significance and applications of heme *c* proteins and peptides. *Acc Chem Res* **48**, 1845-1852

22. Liu, J., Chakraborty, S., Hosseinzadeh, P., Yu, Y., Tian, S., Petrik, I., Bhagi, A., and Lu, Y. (2014) Metalloproteins Containing Cytochrome, Iron–Sulfur, or Copper Redox Centers. *Chemical reviews* **114**, 4366-4469

23. Hartshorne, R. S., Kern, M., Meyer, B., Clarke, T. A., Karas, M., Richardson, D. J., and Simon, J. (2007) A dedicated haem lyase is required for the maturation of a novel bacterial cytochrome *c* with unconventional covalent haem binding. *Molecular microbiology* **64**, 1049-1060

24. Aragao, D., Frazao, C., Sieker, L., Sheldrick, G. M., LeGall, J., and Carrondo, M. A. (2003) Structure of dimeric cytochrome c_3 from *Desulfovibrio gigas* at 1.2 Å resolution. *Acta Crystallogr D Biol Crystallogr* **59**, 644-653

25. Kleingardner, J. G., and Bren, K. L. (2011) Comparing substrate specificity between cytochrome *c* maturation and cytochrome *c* heme lyase systems for cytochrome *c* biogenesis. *Metallomics* **3**, 396-403

26. Ishida, M., Dohmae, N., Shiro, Y., Oku, T., Iizuka, T., and Isogai, Y. (2004) Design and synthesis of de novo cytochromes *c*. *Biochemistry* **43**, 9823-9833

27. Moore, G., and Pettigrew, G. W. (1990) *Cytochromes c. Evolutionary, Structural and Physicochemical Aspects*, 1 ed., Springer-Verlag Berlin Heidelberg

28. Palmer, G. (1985) The electron paramagnetic resonance of metalloproteins. *Biochem Soc Trans* **13**, 548-560

29. Upadhyay, A. K., Petasis, D. T., Arciero, D. M., Hooper, A. B., and Hendrich, M. P. (2003) Spectroscopic characterization and assignment of reduction potentials in the tetraheme cytochrome *c*554 from *Nitrosomonas europaea*. *J Am Chem Soc* **125**, 1738-1747

30. Andersson, K. K., Lipscomb, J. D., Valentine, M., Munck, E., and Hooper, A. B. (1986) Tetraheme cytochrome *c*554 from *Nitrosomonas europaea*. Heme-heme interactions and ligand binding. *The Journal of biological chemistry* **261**, 1126-1138

31. Zhong, F., and Pletneva, E. V. (2018) Ligation and Reactivity of Methionine-Oxidized Cytochrome *c*. *Inorganic chemistry* **57**, 5754-5766

32. Ubbink, M., Campos, A. P., Teixeira, M., Hunt, N. I., Hill, H. A., and Canters, G. W. (1994) Characterization of mutant Met100Lys of cytochrome *c*550 from *Thiobacillus versutus* with lysine-histidine heme ligation. *Biochemistry* **33**, 10051-10059

33. Zhong, F., Lisi, G. P., Collins, D. P., Dawson, J. H., and Pletneva, E. V. (2014) Redox-dependent stability, protonation, and reactivity of cysteine-bound heme proteins. *Proc Natl Acad Sci U S A* **111**, E306-315

34. Amacher, J. F., Zhong, F., Lisi, G. P., Zhu, M. Q., Alden, S. L., Hoke, K. R., Madden, D. R., and Pletneva, E. V. (2015) A Compact Structure of Cytochrome *c* Trapped in a

Lysine-Ligated State: Loop Refolding and Functional Implications of a Conformational Switch. *J Am Chem Soc* **137**, 8435-8449

35. Motomura, T., Suga, M., Hienerwadel, R., Nakagawa, A., Lai, T.-L., Nitschke, W., Kuma, T., Sugiura, M., Boussac, A., and Shen, J.-R. (2017) Crystal structure and redox properties of a novel cyanobacterial heme-protein with a His/Cys heme axial ligation and a per-arnt-sim (PAS)-like domain. *Journal of Biological Chemistry*

36. Cheesman, M. R., Little, P. J., and Berks, B. C. (2001) Novel heme ligation in a *c*-type cytochrome involved in thiosulfate oxidation: EPR and MCD of SoxAX from Rhodovulum sulfidophilum. *Biochemistry* **40**, 10562-10569

37. Brennan, L., Turner, D. L., Fareleira, P., and Santos, H. (2001) Solution structure of Methylophilus methylotrophus cytochrome *c″*: insights into the structural basis of haem-ligand detachment. *Journal of molecular biology* **308**, 353-365

38. Butt, W. D., and Keilin, D. (1962) Absorption Spectra and Some Other Properties of Cytochrome *c* and of Its Compounds with Ligands. *Proceedings of the Royal Society of London. Series B, Biological Sciences* **156**, 429-458

39. Hoshino, M., Ozawa, K., Seki, H., and Ford, P. C. (1993) Photochemistry of nitric oxide adducts of water-soluble iron(III) porphyrin and ferrihemoproteins studied by nanosecond laser photolysis. *Journal of the American Chemical Society* **115**, 9568-9575

40. Haroon, M. F., Hu, S., Shi, Y., Imelfort, M., Keller, J., Hugenholtz, P., Yuan, Z., and Tyson, G. W. (2013) Anaerobic oxidation of methane coupled to nitrate reduction in a novel archaeal lineage. *Nature* **500**, 567-570

41. Ettwig, K. F., Zhu, B., Speth, D., Keltjens, J. T., Jetten, M. S., and Kartal, B. (2016) Archaea catalyze iron-dependent anaerobic oxidation of methane. *Proc Natl Acad Sci U S A*

42. Khmelenina, V. N., Colin Murrell, J., Smith, T. J., and Trotsenko, Y. A. (2018) Physiology and Biochemistry of the Aerobic Methanotrophs. in *Aerobic Utilization of*

Hydrocarbons, Oils and Lipids (Rojo, F. ed.), Springer International Publishing, Cham. pp 1-25

43. Kartal, B., Geerts, W., and Jetten, M. S. M. (2011) Cultivation, Detection, and Ecophysiology of Anaerobic Ammonium-Oxidizing Bacteria. in *Methods in Enzymology. Research on Nitrification and Related Processes, part A.* (Klotz, M. G. ed.), Academic Press, Elsevier. pp 89-109

44. Laemmli, U. K. (1970) Cleavage of structural proteins during the assembly of the head of bacteriophage T4. *Nature* **227**, 680-685

45. Baymann, F., Moss, D. A., and Mäntele, W. (1991) An electrochemical assay for the characterization of redox proteins from biological electron transfer chains. *Analytical biochemistry* **199**, 269-274

46. Moffet, D. A., Foley, J., and Hecht, M. H. (2003) Midpoint reduction potentials and heme binding stoichiometries of de novo proteins from designed combinatorial libraries. *Biophysical chemistry* **105**, 231-239

47. Petersen, T. N., Brunak, S., von Heijne, G., and Nielsen, H. (2011) SignalP 4.0: discriminating signal peptides from transmembrane regions. *Nat Methods* **8**

48. Edgar, R. C. (2004) MUSCLE: multiple sequence alignment with high accuracy and high throughput. *Nucleic Acids Res* **32**, 1792-1797

49. Farhoud, M. H., Wessels, H. J. C. T., Steenbakkers, P. J. M., Mattijssen, S., Wevers, R. A., Van Engelen, B. G., Jetten, M. S. M., Smeitink, J. A., Van Den Heuvel, L. P., and Keltjens, J. T. (2005) Protein complexes in the archaeon *Methanothermobacter thermautotrophicus* analyzed by blue native/SDS-PAGE and mass spectrometry. *Molecular & Cellular Proteomics* **4**, 1653-1663

50. Bradford, M. M. (1976) A rapid and sensitive method for the quantitation of microgram quantities of protein utilizing the principle of protein-dye binding. *Analytical biochemistry* **72**, 248-254

51. Berry, E. A., and Trumpower, B. L. (1987) Simultaneous determination of hemes *a*, *b*, and *c* from pyridine hemochrome spectra. *Analytical biochemistry* **161**, 1-15

52. Na, S.-I., Kim, Y. O., Yoon, S.-H., Ha, S.-m., Baek, I., and Chun, J. (2018) UBCG: Up-to-date bacterial core gene set and pipeline for phylogenomic tree reconstruction. *Journal of Microbiology* **56**, 280-285

53. Letunic, I., and Bork, P. (2019) Interactive Tree Of Life (iTOL) v4: recent updates and new developments. *Nucleic Acids Research* **47**, W256-W259

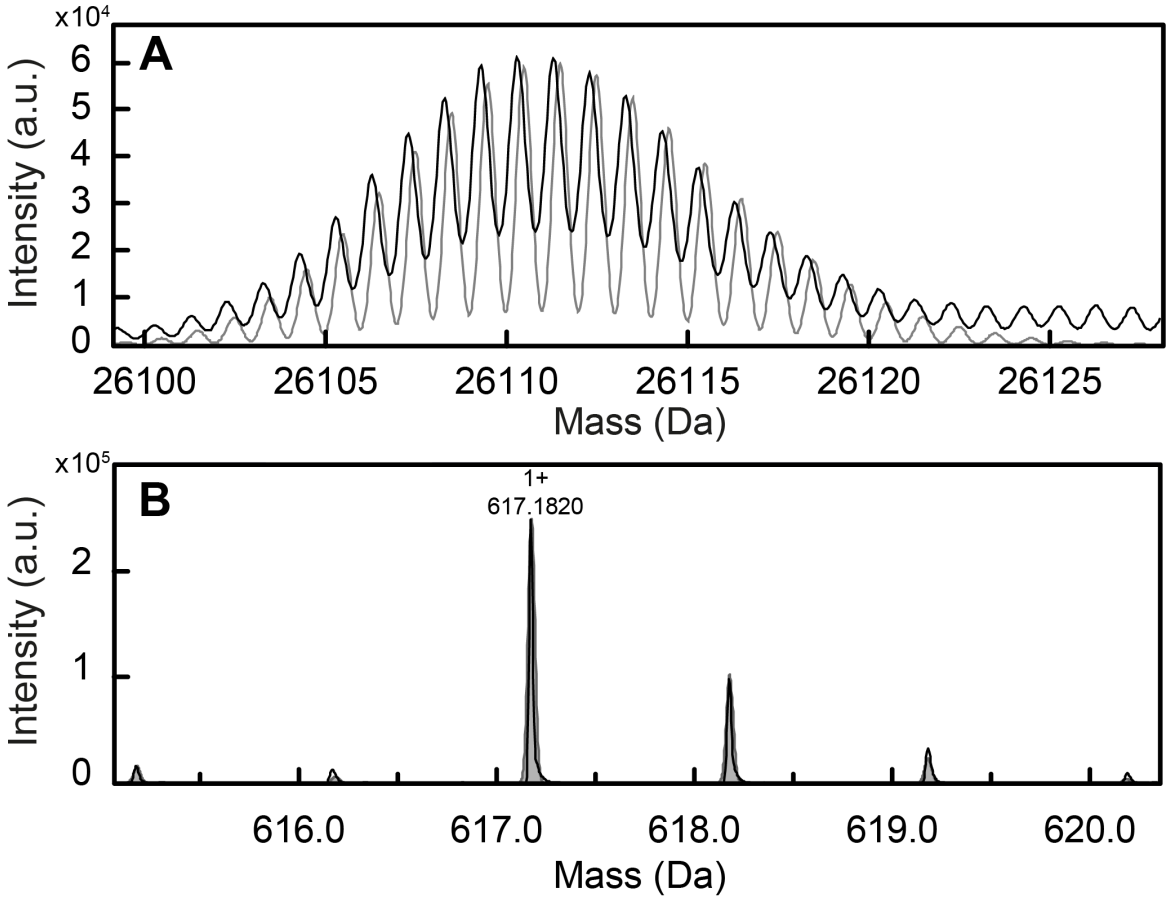

Figure 1: Mass spectrometry analysis of intact KsTH

A) Tandem mass spectrometry analysis of the intact protein established a molecular mass of 26095.2744 Da for the monoisotopic species. The theoretical value of the apoprotein without the N-terminal targeting sequence (aa: 1-29) is 23634.79 Da. **B)** Collision–induced dissociation tandem mass spectrometry (CID MS/MS) identified only one dominant fragment ion of 617.18 $[M+H]^{1+}$that matched the simulated isotope envelope of Fe-protoporphyrin IX, indicating the absence of other cofactors.

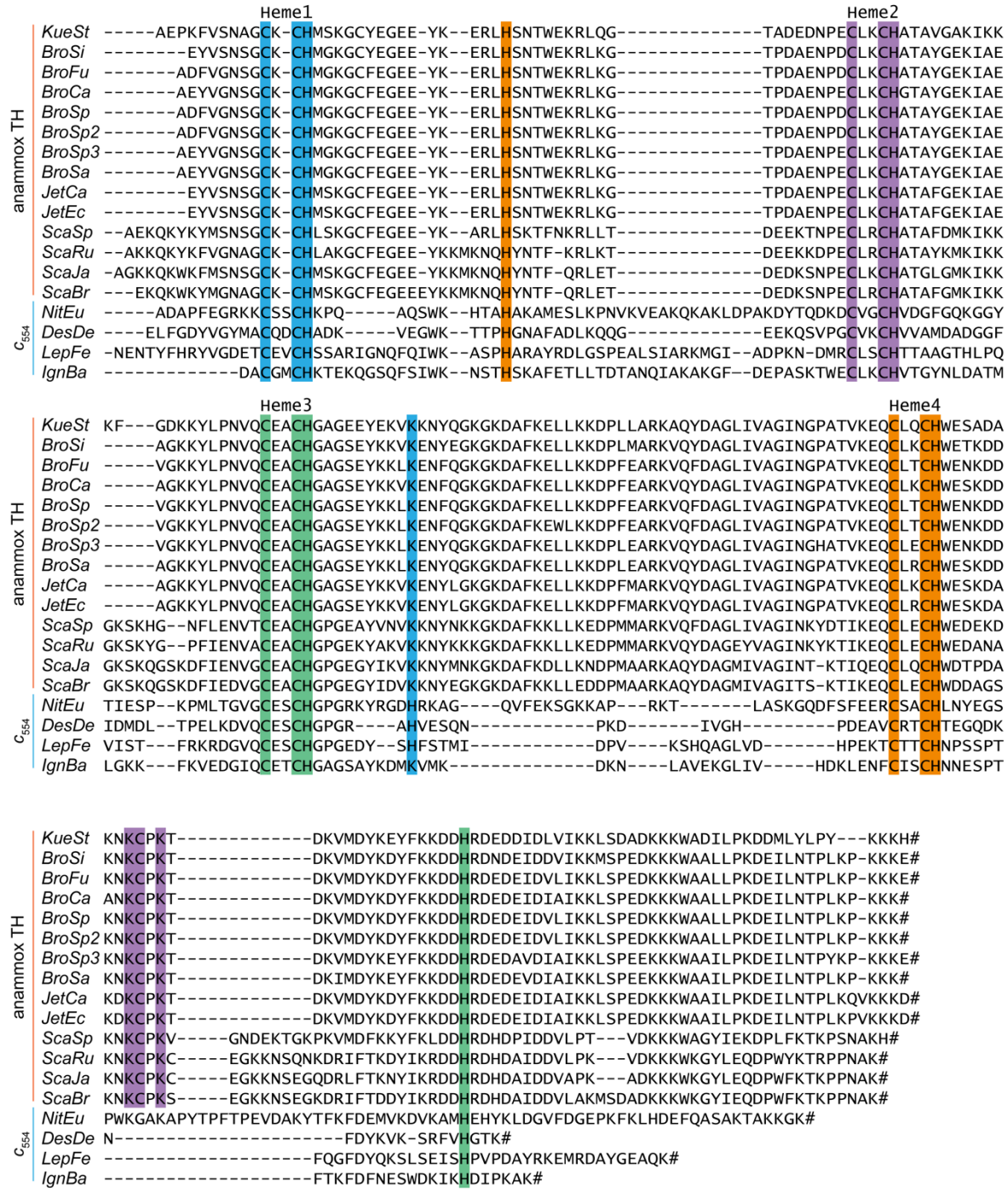

Figure 2: Sequence alignment of anammox TH sequences and cytochrome c_{554}

Heme-binding motifs and putative sixth ligands of heme 1 (blue), 2 (purple), 3 (green) and 4 (orange) are highlighted. Tetraheme (TH) sequences and cytochrome c_{554} (c554), and the corresponding accession numbers are as follows: KueSt; Candidatus Kuenenia stuttgartiensis (WP_099326586.1), BroSi; Candidatus Brocadia sinica (KXK27878.1), BroFu; Candidatus Brocadia fulgida (KKO18049.1), BroCa; Candicatus Brocadia caroliniensis (OOP55820.1),

BroSp; Candidatus Brocadia sp. (RIJ93553.1), BroSp1; Candidatus Brocadia sp. UTAMX1 (OQZ04649.1), BroSp2; Candidatus Brocadia sp. UTAMX2 (OQY97542.1), BroSP3; Candidatus Brocadia sp. BROELEC01 (RZV58464.1), BroSa; Candidatus Brocadia sapporoensis (WP_070066581.1), JetCa; Candidatus Jettenia caeni (JGAB63755.1), JetEc; Candidatus Jettenia ecosi (TLD42491.1), ScaSp; Candidatus Scalindua sp. SCAELEC01 (RZV91387.1), ScaRu; Candidatus Scalindua rubra (ODS33861.1), ScaJa; Candidatus Scalindua japonica (WP_096896270.1), ScaBr; Candidatus Scalindua brodae (KHE90513.1), NitEu; Nitrosomonas europaea (Q57142), DesDe; Desulfovibrio desulfuricans (F0JDN8), LepFe; Leptospirillum ferriphilum (J9ZB89), IgnBa; Ignavibacteria bacterium (A0A1J5F6W4). Genome sequences corresponding to TH_ScaBr and TH_JetEc were used to manually curate the amino acid sequences in order to account for a frame shift, and different assignment of the start codon, respectively.

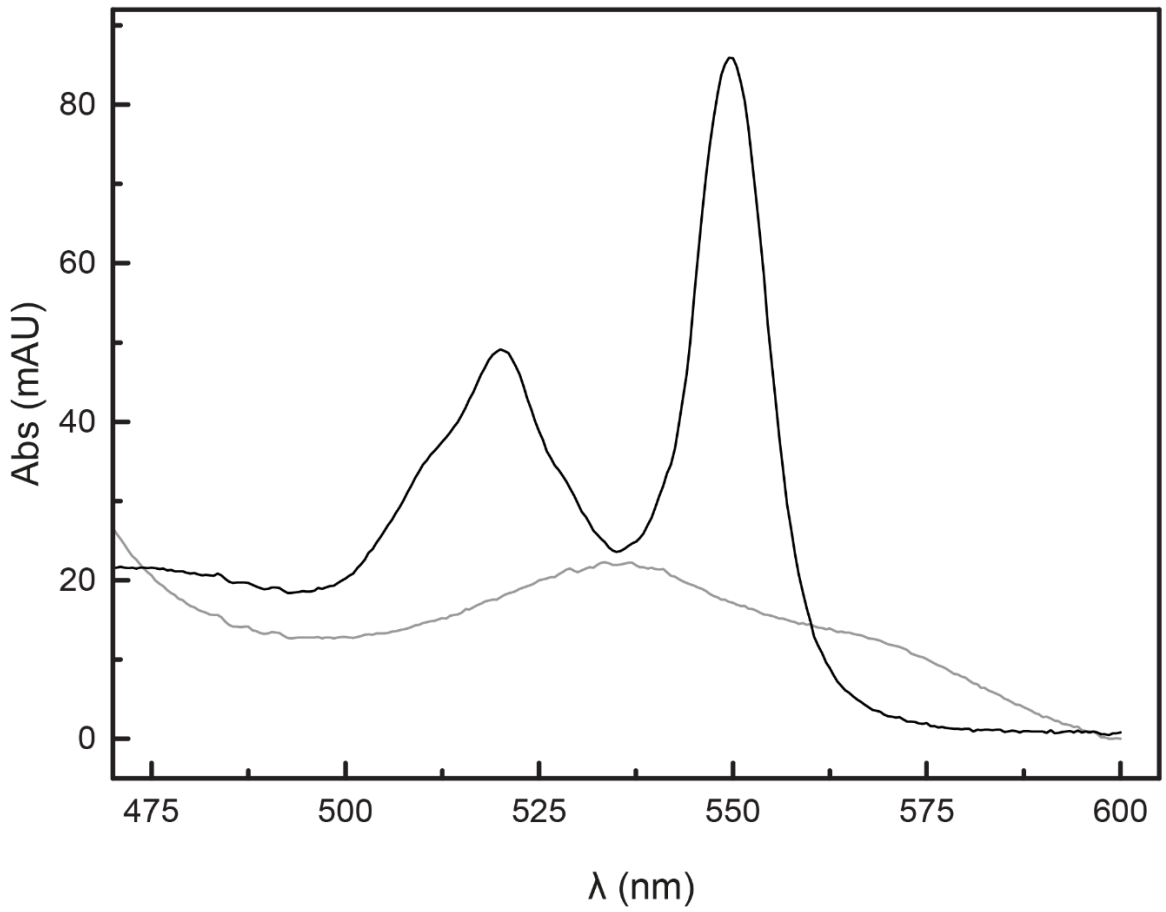

Figure 3: Pyridine hemochromogen assay

The Q-bands of the spectrum of reduced alkaline bis–pyridine adduct of KsTH revealed absorbance maxima corresponding to the heme attachment via two thioether bonds.

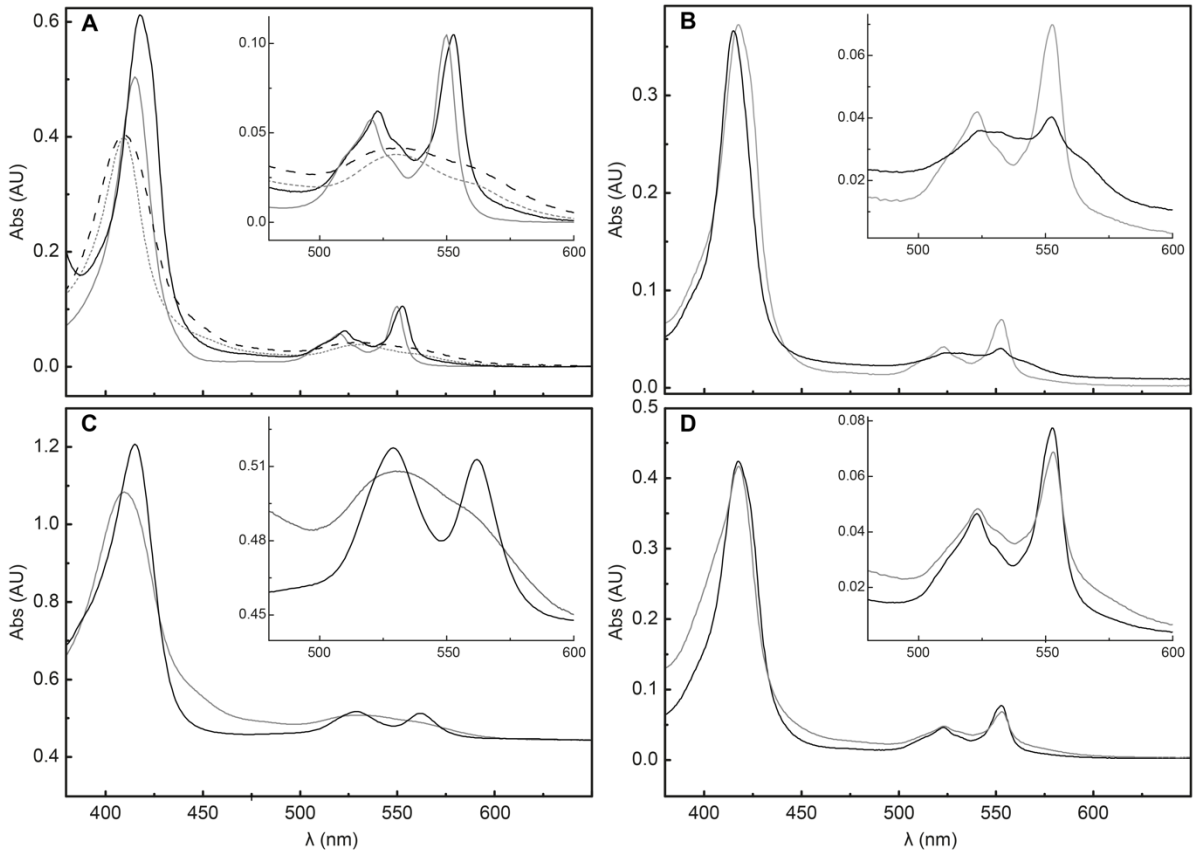

Figure 4: optical spectra of KsTH

A) Spectra of KsTH (black lines) and horse heart cytochrome c (grey lines) in the oxidized state as prepared (dashed lines) and after dithionite reduction (solid lines). **B)** Spectrum of reduced KsTH before (black line) and after addition of CO (grey line). **C)** Spectrum of oxidized KsTH before (black line) and after addition of addition of NO (grey line). **D)** Spectrum of reduced KsTH before (black line) and after addition of NO (grey line). Each inset shows a close-up view of the Q-band region.

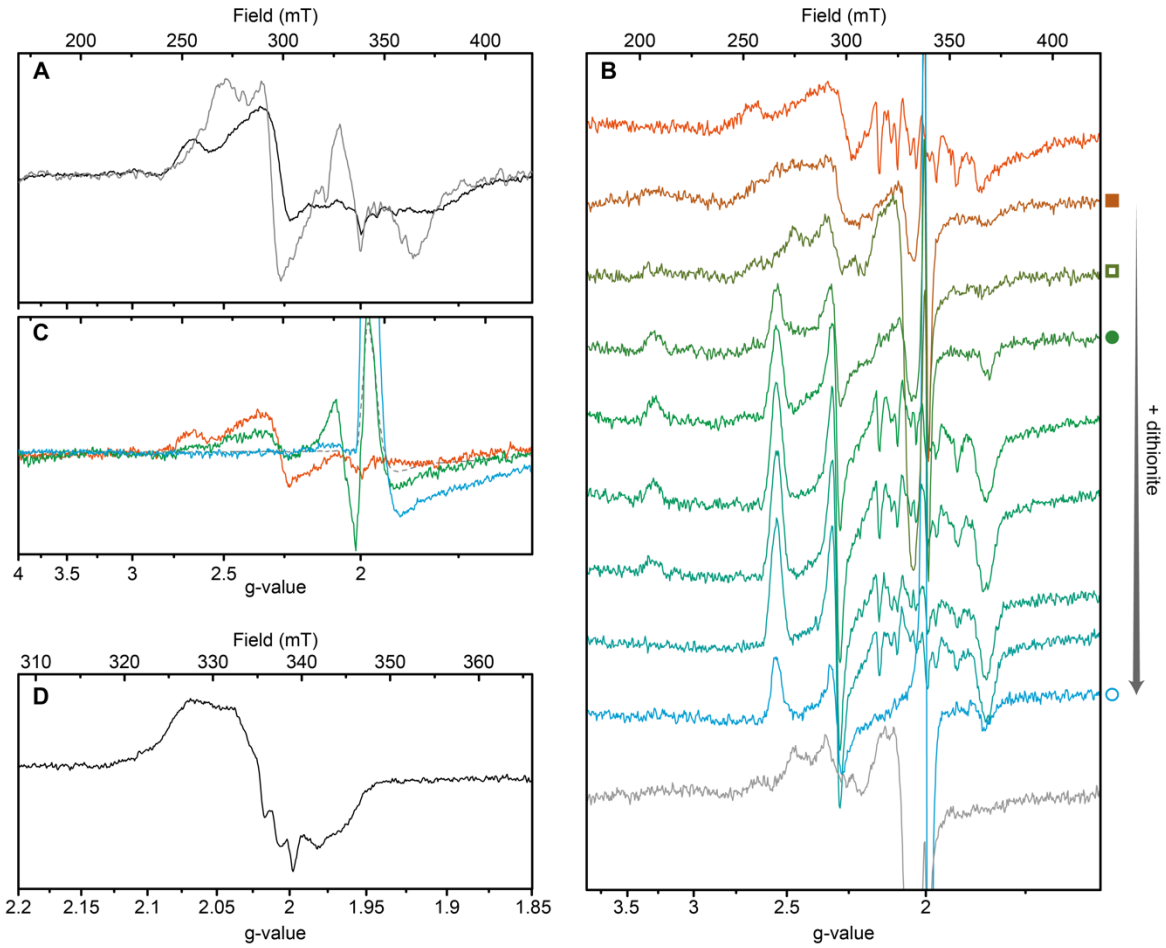

Figure 5: EPR spectra of KsTH

A) Spectra recorded at a temperature of 15K, microwave power of 1mW (black line) and at a temperature of 100K and a microwave power of 64mW (grey line), modulation amplitude 0 Gauss; spectra were normalized to temperature and microwave power. **B)** Spectra recorded after successive addition of dithionite in the absence and in the presence of mediators (denoted with symbols adjacent to the corresponding lines). In presence of mediators, a redox electrode was used to monitor the potential: closed square: -210 mV, open square: -225 mV, closed circle: -280 mV, open circle: -410 mV (all potentials are *vs.* SHE). Addition of ferricyanide to the dithionite reduced sample without mediators resulted in the spectrum that is shown as a grey line. Signals around g=2 stem from Mn contamination in the sample without mediators and from contaminating Cu and radical signals of the mediators in the other samples; temperature 15 K, microwave power 1 mW, modulation amplitude 10 Gauss. **C)** Spectra recorded on KsTH

(orange line) and after addition of NO-saturated water to a final concentration of 60 µM (green line) and 600 µM (blue); NO-saturated water (dashed grey line), temperature 15 K, microwave power 1 mW, modulation amplitude 10 Gauss; **D)** Spectrum recorded after addition of dithionite and nitrite, temperature 50 K, microwave power 6.4 mW, modulation amplitude 3 Gauss.

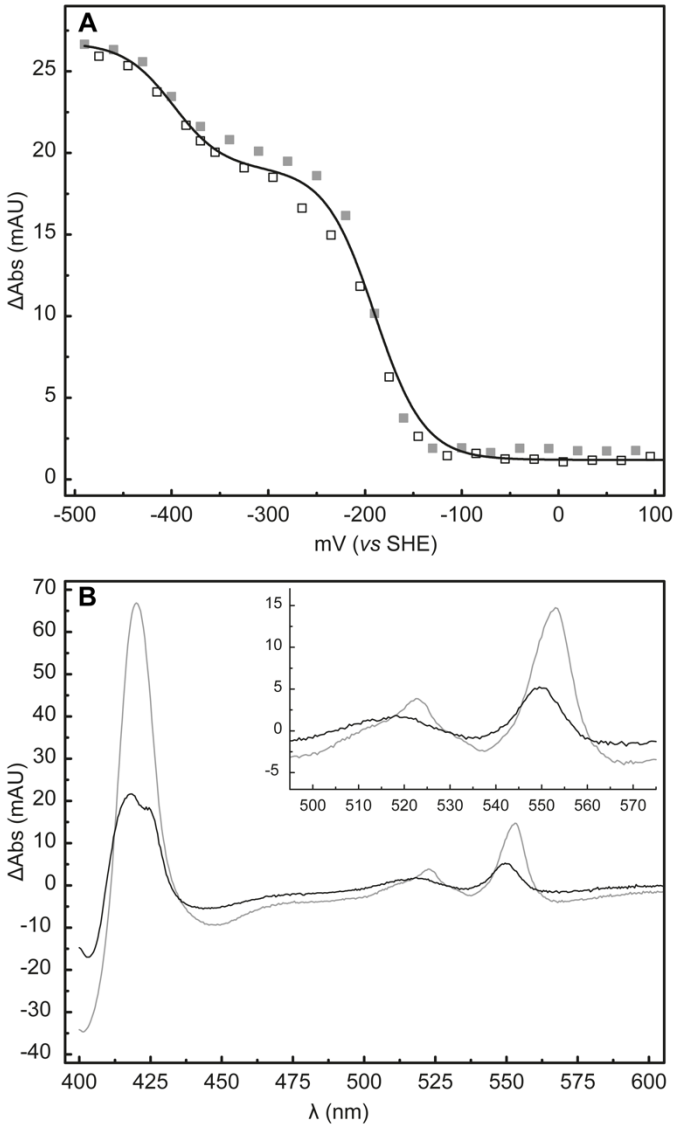

Figure 6: Optical redox titration

Using an optically transparent thin layer electrochemical cell, redox potentials in the range from +290 to -475 mV were applied in oxidizing and reducing directions. After equilibration absorbance chances were monitored. **A)** A sum of two n=1 Nernst equations was fitted to the

difference in absorbance between 552-565 nm (solid black line), resulting in midpoint potentials of -190±20 mV and -400±20 mV, respectively. Open and closed circles represent data recorded in the oxidative or reducing direction, respectively. **B)** Difference spectra corresponding to the redox transition at -400 mV (black line) and -190 mV (grey line).

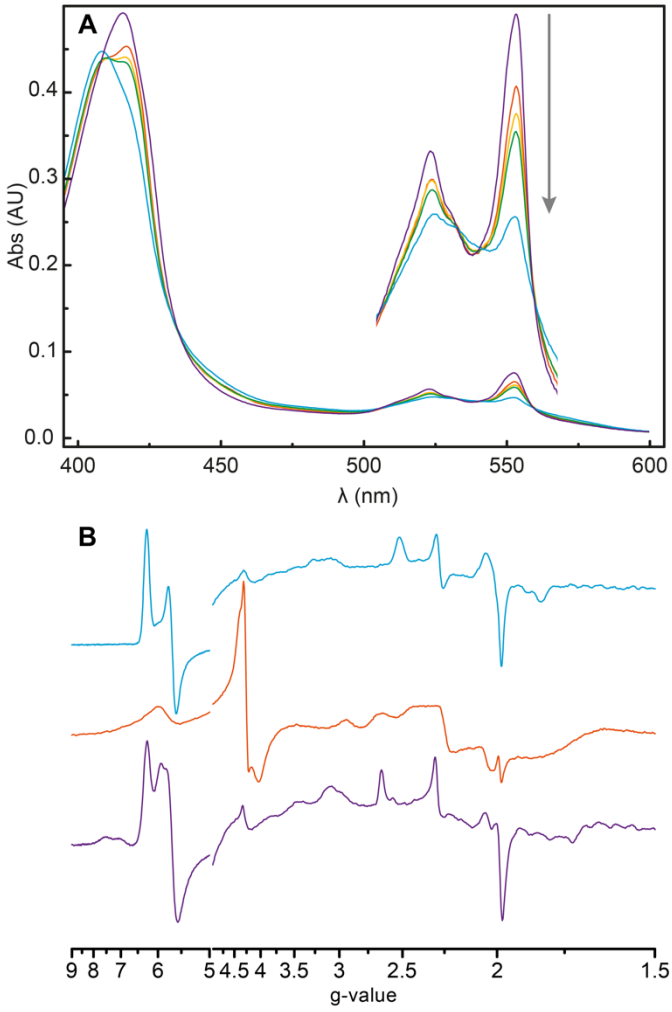

Figure 7: Redox interaction between KsTH and hydrazine synthase

A) Combined spectrum of reduced KsTH and oxidized HZS (5:1 stoichiometry) before mixing (purple) and 0 (red), 3 (yellow), 6 (green), and 12 (blue) minutes after mixing. The inset shows a detailed view of the α band region. **B)** EPR spectra of a mixture of reduced KsTH with oxidized HZS in a 1:1 stoichiometry (blue) and of as–isolated, fully oxidized KsTH (orange) and HZS (purple). Spectra were recorded at 13 K, 2 mW microwave power, and with 20 dB modulation amplitude. The KsTH spectrum shows in this experiment a signal at g=2.95 that was not present on other KsTH preparations and may stem from a contaminant.

Figure 8. An unrooted phylogenetic tree showing taxa that code for amino acid sequences of *c*-type cytochromes featuring a contracted heme-binding motif in addition to at least one conventional CxxCH motif. Alignment was performed using a concatenated set of 92 conserved phylogenetic markers retrieved using the UBCG pipeline.

Discovery of a functional, contracted heme-binding motif within a multiheme cytochrome

Christina Ferousi, Simon Lindhoud, Frauke Baymann, Eric R. Hester, Joachim Reimann and Boran Kartal

J. Biol. Chem. published online October 3, 2019
